Monthly Notices
of the
ROYAL ASTRONOMICAL SOCIETY

MNRAS **481,** 1115–1125 (2018)
Advance Access publication 2018 September 3

doi:10.1093/mnras/sty2350

Constraining the microlensing effect on time delays with a new time-delay prediction model in H_0 measurements

Geoff C.-F. Chen,[1]★ James H. H. Chan,[2] Vivien Bonvin,[2] Christopher D. Fassnacht,[1] Karina Rojas,[3]† Martin Millon,[2] Fred Courbin,[2] Sherry H. Suyu,[4,5,6] Kenneth C. Wong,[7] Dominique Sluse,[8] Tommaso Treu,[9] Anowar J. Shajib,[9] Jen-Wei Hsueh,[1] David J. Lagattuta,[10] Léon V. E. Koopmans,[11] Simona Vegetti[4] and John P. McKean[11,12]

[1]*Department of Physics, University of California, Davis CA 95616, USA*
[2]*Institute of Physics, Laboratoire d'Astrophysique, Ecole Polytechnique Fédérale de Lausanne (EPFL), Observatoire de Sauverny, CH-1290 Versoix, Switzerland*
[3]*Instituto de Física y Astronomía, Universidad de Valparaíso, Avda. Gran Bretaña 1111, Playa Ancha, Valparaíso 2360102, Chile*
[4]*Max Planck Institute for Astrophysics, Karl-Schwarzschild-Strasse 1, D-85740 Garching, Germany*
[5]*Institute of Astronomy and Astrophysics, Academia Sinica (ASIAA), PO Box 23-141, Taipei 10617, Taiwan*
[6]*Physik-Department, Technische Universität München, James-Franck-Straße 1, 85748 Garching, Germany*
[7]*National Astronomical Observatory of Japan, 2-21-1 Osawa, Mitaka, Tokyo 181-8588, Japan*
[8]*STAR Institute, Quartier Agora – Allée du six Août, 19c, B-4000 Liége, Belgium*
[9]*Department of Physics and Astronomy, University of California, Los Angeles CA 90095-1547, USA*
[10]*CRAL, Observatoire de Lyon, Universit Lyon 1, 9 Avenue Ch. Andr, F-69561 Saint Genis Laval Cedex, France*
[11]*Kapteyn Astronomical Institute, University of Groningen, PO Box 800, NL-9700 AV Groningen, the Netherlands*
[12]*Netherlands Institute for Radio Astronomy (ASTRON), PO Box 2, NL-7990 AA Dwingeloo, the Netherlands*

Accepted 2018 August 25. Received 2018 August 11; in original form 2018 April 28

ABSTRACT

Time-delay strong lensing provides a unique way to directly measure the Hubble constant (H_0). The precision of the H_0 measurement depends on the uncertainties in the time-delay measurements, the mass distribution of the main deflector(s), and the mass distribution along the line of sight. Tie & Kochanek have proposed a new microlensing effect on time delays based on differential magnification of the coherent accretion disc variability of the lensed quasar. If real, this effect could significantly broaden the uncertainty on the time-delay measurements by up to 30 per cent for lens systems such as PG 1115+080, which have relatively short time delays and monitoring over several different epochs. In this paper we develop a new technique that uses the cosmological time-delay ratios and simulated microlensing maps within a Bayesian framework in order to limit the allowed combinations of microlensing delays and thus to lessen the uncertainties due to the proposed effect. We show that, under the assumption of Tie & Kochanek, the uncertainty on the time-delay distance ($D_{\Delta t}$, which is proportional to $1/H_0$) of the short time-delay (∼18 d) lens, PG 1115+080, increases from ∼7 per cent to ∼10 per cent by simultaneously fitting the three time-delay measurements from the three different data sets across 20 yr, while in the case of the long time-delay (∼90 d) lens, the microlensing effect on time delays is negligible as the uncertainty on $D_{\Delta t}$ of RXJ 1131−1231 only increases from ∼2.5 per cent to ∼2.6 per cent.

Key words: gravitational lensing: micro – distance scale – methods: data analysis.

1 INTRODUCTION

The standard flat lambda cold dark matter (ΛCDM) model has become a concordance cosmological model, which assumes spatial flatness, a matter content dominated by cold dark matter, and an

★ E-mail: chfchen@ucdavis.edu
† LSSTC Data Science Fellow

accelerated expansion caused by dark energy (Planck Collaboration XIII 2016). Intriguingly, even though the standard flat ΛCDM model provides an excellent fit to various large-scale observables, including the cosmic microwave background (CMB) and baryon acoustic oscillations (BAO; Komatsu et al. 2011; Hinshaw et al. 2013), the current $\sim 3\sigma$ tension between direct measurements of H_0 and that inferred from *Planck* data based on the flat ΛCDM model may indicate new physics beyond the standard cosmological model (Riess et al. 2016; Freedman 2017). Therefore, to clarify whether this tension is due to systematics, multiple independent methods with precise (1 per cent or better) and accurate H_0 measurements are crucial for testing the possible hidden biases in any individual method (e.g. Suyu 2012; Weinberg et al. 2013).

Time-delay strong lensing (TDSL), which uses gravitational lens systems in which a foreground galaxy produces multiple images of a variable background object such as a quasar, is a powerful technique for measuring H_0. Compared to Type Ia supernovae, which need to be calibrated either by distance ladder techniques (Riess et al. 1998) or by an inverse distance ladder from BAO and CMB to yield H_0 (Aubourg et al. 2015), TDSL is not only a completely independent method but also a one-step way to probe H_0. The measurements are obtained by constraining the combined cosmological distances (or so-called time-delay distance, $D_{\Delta t}$), which are mostly sensitive to H_0 (see the review by Treu & Marshall 2016). While this method was proposed by Refsdal (1964) over fifty years ago, it is only in the last fifteen years that robust measurements of high enough precision have been achieved, recently yielding a 3.8 per cent accurate measurement of H_0 based on the time-delay measurements in three lenses (Bonvin et al. 2017).

The methodology of TDSL relies on three inputs for each lens: (1) multi-year lens monitoring programs to measure high-precision time delays (e.g. Fassnacht et al. 2002; Eulaers et al. 2013; Rathna Kumar et al. 2013; Tewes, Courbin & Meylan 2013a; Bonvin et al. 2017; Courbin et al. 2018), (2) high-resolution imaging and stellar kinematics to determine the mass distribution in the lensing galaxy (e.g. Treu & Koopmans 2002; Koopmans et al. 2003; Suyu et al. 2010; Wong et al. 2017), and (3) spectroscopy and multiband imaging to provide an inference of the mass distribution along the line of sight of the lens system (Suyu et al. 2010; Fassnacht, Koopmans & Wong 2011; Rusu et al. 2017; Tihhonova et al. 2018). The error budget of each component, assuming they are independent, can be approximately translated to the H_0 error budget by $\sigma^2_{H_0}/H_0^2 \propto (\sigma^2_{\delta t}/\delta t^2 + \sigma^2_{\kappa} + \sigma^2_{\rm los})/N$, where $\sigma_{\delta t}$, σ_{κ}, and $\sigma_{\rm los}$ are the uncertainties on the time-delay measurements, the mass distribution of the main deflector(s), and the mass along the line of sight, respectively, and N is the number of lenses. Since each lens is independent of another lens, one can keep pushing down the precision of the H_0 measurements by combining more and more lenses until one hits the systematic error floor in any individual component. Current large sky surveys combining with numerical lens-finding techniques (e.g. Joseph et al. 2014; Agnello 2017; Avestruz et al. 2017; Ostrovski et al. 2017; Petrillo et al. 2017; Lanusse et al. 2018) have already shown promising results and discovered many new lenses (e.g. Lin et al. 2017; Schechter et al. 2017; Agnello et al. 2018; Ostrovski et al. 2018; Williams et al. 2018). Furthermore, Oguri & Marshall (2010) forecast that we will discover thousands of lensed quasars with the Large Synoptic Survey Telescope. Hence, a 1 per cent H_0 measurement is a realistic expectation in the near future (e.g. Jee, Komatsu & Suyu 2015; Jee et al. 2016; de Grijs et al. 2017; Jee et al. 2018 submitted; Shajib, Treu & Agnello 2018; Suyu et al. 2018) if we can control the systematic effects in each error budget to a subpercent level.

There are in general two ways to reveal systematic uncertainties. The first is performing a mock data set challenge: Mock data sets that mimic real data are created and then modellers analyse the data sets and compare their results with truth to reveal any systematic effect in their modelling algorithms. For example, the public time-delay challenge (TDC; Dobler et al. 2013; Liao et al. 2015) aimed to examine the accuracy of different time-delay curve-fitting algorithms. The main purpose of the TDC was to understand how well we can control systematics on $\sigma_{\delta t}$. The conclusion was that if the measured time delay is the standard cosmological delay (see the definition in equation 7) used in all lens models, it is feasible to measure accurate and precise time delays within 1 per cent (Tewes et al. 2013b; Liao et al. 2015; Bonvin et al. 2017). Similarly, the ongoing public time-delay lens-modelling challenge (TDLMC; Ding et al. 2018) aims to test the accuracy of lens imaging modelling algorithms based on different source reconstruction techniques (e.g. Warren & Dye 2003; Koopmans 2005; Vegetti & Koopmans 2009; Oguri 2010; Birrer, Amara & Refregier 2015; Nightingale & Dye 2015). Additionally, the TDLMC may shed light on how critical the mass-sheet transformation (MST), a special case of source-position transformation, is (Falco, Gorenstein & Shapiro 1985; Schneider & Sluse 2013, 2014; Xu et al. 2016; Birrer et al. 2017). All in all, the goal of the TDLMC is to understand how well we can control the systematic effects on σ_{κ}. In addition, Birrer et al. (2015) used mock data to study whether we can use lens imaging to detect small perturbations on σ_{κ}, while Chen et al. (2016) used mock data to study the impact of the unstable point spread function on σ_{κ} when using adaptive optics imaging to study H_0. However, it is difficult for mock data set challenges to reveal the systematics caused by unknown physical phenomena because the mock data only include known processes.

The second method to assess systematic effects is to study physical processes that have not been previously considered. For example, Tie & Kochanek (2018; hereafter TK18) have questioned the use of measured time delays in cosmography, by showing that, under the assumption of the 'lamp-post' model for accretion discs and differential magnification of the disc stars in the lensing galaxy (i.e. microlensing; Wambsganss 2006), the measured time delays may introduce a bias in the inferred value of H_0. Under this assumed disc model, regions of the accretion disc that are separated by distances of the order of of light days vary in a coherent manner in response to activity in the centre of the disc. Differential magnification of portions of such a disc can introduce a phase delay due to the distance from the centre of the disc, and can shift the time-delay light curves by up to days depending on the accretion disk configuration and the microlensing pattern (see more description in Section 2). Since each lensed image has a different microlensing pattern, the sum of this proposed microlensing time-delay effect for any pair of lensed images can be non-zero. Therefore, the time delays we measure are not only the cosmological time delays but a combination of cosmological time delays and microlensing time delays,

$$\Delta t_{\rm measured} = \Delta t_{\rm cosmological} + \Delta t_{\rm microlensing}. \quad (1)$$

This effect, under certain assumptions, can significantly broaden the uncertainty on time-delay measurements, since it is embedded in the time-delay light curves (see fig. 10 in TK18). Although long-term monitoring can partially average out and mitigate this microlensing effect on time delays, the non-zero mean cannot be removed (see table 2 in TK18). Thus, TK18 have claimed that the current uncertainty of H_0 measurements from TDSL could potentially be underestimated and biased.

Table 1. The κ, γ, and $\kappa_\star/\kappa$ at each lensed image position in PG 1115+080 from the best fit of the macro model (Chen et al. 2018b, in prep). Values for RXJ 1131−1231 are taken from TK18.

Lens	Image	κ	γ	$\kappa_\star/\kappa$
PG 1115+080	A_1	0.424	0.491	0.259
	A_2	0.451	0.626	0.263
	B	0.502	0.811	0.331
	C	0.356	0.315	0.203

Although the effect suggested by TK18 depends on an AGN variability model that is not yet well constrained observationally, in this paper we conservatively assume that this effect exists and develop a new technique to mitigate its consequences. We use a time-delay prediction model that incorporates the information from the cosmological time-delay ratio, which was first proposed by Keeton & Moustakas (2009),[1] as well as the information from the microlensing time-delay maps. In Section 2, we show the microlensing time-delay maps resulting from different source configurations. In Section 3, we demonstrate how to properly infer $D_{\Delta t}$ by including the new microlensing effects using Bayesian inference.[2] We show the time-delay modelling results of PG 1115+080 and RXJ 1131−1231 in Section 4, and summarize in Section 5. Note that, throughout the paper,[3] we use the phrase 'microlensing time-delay effect' to refer to the microlensing effect on time delays proposed by TK18, and use 'microlensing magnification effect' to refer to the 'standard' microlensing magnification of the image fluxes.

2 MICROLENSING TIME-DELAY MAPS

In order to assess the magnitude of the microlensing time-delay effect and to test our procedure, we need to create realizations of microlensing maps that are due to the stars in the lensing galaxies. Rather than showing magnification, as is typical when showing microlensing realizations, these maps show the additional time delays introduced by the microlensing, under the assumption that the lamp-post model (see TK18) is correct. The details of creating the microlensing time-delay map for PG 1115+080 can be found in Bonvin et al. 2018 (hereafter B18). We summarize the key information in the following. We follow TK18 to produce microlensing time-delay maps at each lensed image position in a lens system given the total convergence (κ), the ratio of stellar convergence to total convergence ($\kappa_\star/\kappa$), and the shear (γ) from the best fit of the macro model (see Table 1 for PG 1115+080 and TK18 for RXJ 1131−1231).[4] We assume a mean mass of the microlenses of $\langle M\rangle = 0.3\,M_\odot$ following the Salpeter mass function with a ratio of the upper to lower masses of $r = 100$ (Kochanek & Dalal 2004), although the choice of the mass function has little influence on our results (B18). We consider a standard thin-disc model (Shakura & Sunyaev 1973) for the accretion disc given an estimated black hole mass, for example, of $1.2\times10^9\,M_\odot$ for PG 1115+080 (Peng et al. 2006). According to TK18, the microlensing screen due to the lensing galaxy may cause differential magnification of the accretion disc region of the background quasar. This can change the relative contributions of different parts of the accretion disc to the integrated flux of the image, and consequently change the average radius at which the variability takes place. There are two main sources of the delay: (1) If the temperature profile (and hence brightness profile) of the disc responds to variations in the centre, which then propagate outward through the accretion disc, the differentially magnified ultraviolet (UV)/optical emission from the disc can shift the light curve to a later time and also change its shape, and (2) if the disc is tilted with respect to the line of sight, then there are extra light travel times from different parts of the disc. We show the time-delay maps in Fig. 1, and list the combinations of different accretion disc sizes ($0.5R_0$, $1R_0$, and $2R_0$), different ϕ (0° and 60°), and different PA (0°, 45°, and 90°), where ϕ[4] and PA represent the inclination and position angle of the disc with respect to the source plane, taken as perpendicular to the observer's line of sight ($\phi = 0$ corresponding to the face-on disc; see TK18 for a detailed explanation of the coordinate system). The probability distribution of the time-delay maps with different combinations can be found in fig. 5 of B18.

3 BAYESIAN INFERENCE

In this section, we describe how we include and constrain the microlensing effects on time delays and properly infer $D_{\Delta t}$ under a Bayesian framework. We denote Δt as the measured time delays in equation (1), d as the lens imaging data, $\tilde{m}_k$ as the microlensing model with a particular accretion disc property k (i.e. a particular combination of disc size, ϕ, and PA), $t_{\tilde{m}_k}$ as the parameters of the extra time delays at each lensed image caused by the microlensing model, $\tilde{M}$ as the macro model that is constrained by the lens imaging, $\xi_{\tilde{M}}$ as the parameters of the macro model, and again $D_{\Delta t}$ as the time-delay distance.

The posterior of $D_{\Delta t}$, $t_{\tilde{m}_k}$, and $\xi_{\tilde{M}}$ is

$$\begin{aligned}&\mathrm{P}(D_{\Delta t}, t_{\tilde{m}_k}, \xi_{\tilde{M}}|\Delta t, d, \tilde{m}_k, \tilde{M})\\ &\quad\propto \mathrm{P}(\Delta t, d|D_{\Delta t}, t_{\tilde{m}_k}, \xi_{\tilde{M}}, \tilde{m}_k, \tilde{M})\\ &\qquad\cdot \mathrm{P}(D_{\Delta t})\mathrm{P}(t_{\tilde{m}_k}|\tilde{m}_k, \tilde{M})\mathrm{P}(\xi_{\tilde{M}}|\tilde{M}),\end{aligned} \tag{2}$$

where $\mathrm{P}(\Delta t, d|D_{\Delta t}, t_{\tilde{m}_k}, \xi_{\tilde{M}}, \tilde{m}_k, \tilde{M})$ is the joint likelihood of the lens and

$$\mathrm{P}(t_{\tilde{m}_k}|\tilde{m}_k, \tilde{M}) = \prod_i^{N_{\rm im}} \mathrm{P}(t_{i,\tilde{m}_k}|\tilde{m}_k, \tilde{M}) \tag{3}$$

is the prior from the time-delay maps in the microlensing model with a particular accretion disc property given the mass distribution from the macro model, $t_{i,\tilde{m}_k}$ are the extra time delays caused by the microlensing effect at the location of each lensed image i, and $N_{\rm im}$ is the number of lensed images. Since the data are independent, we can decouple the joint likelihood as

$$\begin{aligned}&\mathrm{P}(\Delta t, d|D_{\Delta t}, t_{\tilde{m}_k}, \xi_{\tilde{M}}, \tilde{m}_k, \tilde{M})\\ &\quad= \mathrm{P}(\Delta t|D_{\Delta t}, t_{\tilde{m}_k}, \xi_{\tilde{M}}, \tilde{m}_k, \tilde{M})\mathrm{P}(d|\xi_{\tilde{M}}, \tilde{M}).\end{aligned} \tag{4}$$

[1]The extra time delays caused by substructures are negligible (<0.5 d) even when the mass of the substructures is larger than $10^9\,M_\odot$ (see fig. 3 in Keeton & Moustakas 2009; Mao & Schneider 1998).

[2]We use `emcee` (Foreman-Mackey et al. 2013), an MIT licensed pure-PYTHON implementation of Goodman & Weare (2010) Affine Invariant Markov chain Monte Carlo (MCMC) Ensemble sampler, to perform the MCMC analysis. All the chains have converged based on the criteria in Foreman-Mackey et al. (2013).

[3]We use `ChainConsumer`, a package developed by Hinton (2016), to create colour-blind accessible figures.

[4]Note that TK18 and B18 use i to represent the inclination angle.

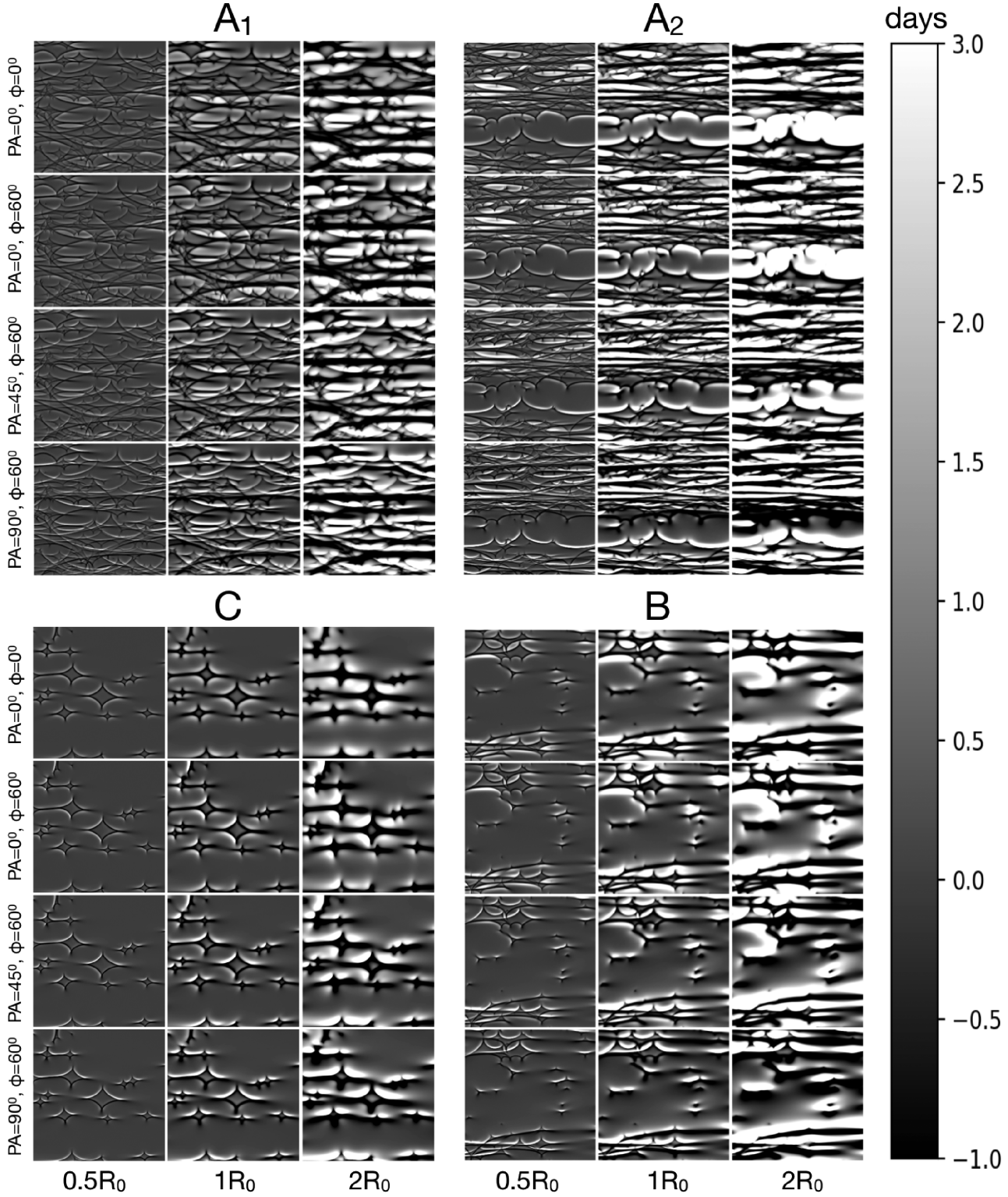

Figure 1. The microlensing time-delay maps for image A_1 (top left-hand panel), A_2 (top right-hand panel), B (bottom right-hand panel), and C (bottom left-hand panel) of PG 1115+080. For each panel, the top row is for a face-on disc and the lower three rows are for a disc inclined by $\phi = 60^\circ$ with position angles of PA $=0^\circ$, 45°, and 90°, respectively. Each column refers to a different source size: (left) $0.5R_0$, (middle) $1R_0$, and (right) $2R_0$, where $R_0 = 1.629 \times 10^{15}$ cm in the Wide Field Imager (WFI) R_c filter (6517.25 Å) for an Eddington ratio of $L/L_E = 0.1$ and a radiative efficiency of $\eta = 0.1$, given an estimated black hole mass of $1.2 \times 10^9\,\mathrm{M}_\odot$ from Peng et al. (2006). All images are on the same scale with the minimum set at -1 d and maximum at +3 d, although certain pixels have delays that fall outside of this range. Black is used for negative delays and white for positive delays. Each map has the size of $20R_{\mathrm{Ein}}$ with a 8192-pixel resolution, where $R_{\mathrm{Ein}} = 3.618 \times 10^{16}$ cm is the Einstein radius of a mean mass of the microlenses, $\langle M \rangle = 0.3\,\mathrm{M}_\odot$.

We can substitute equation (4) into equation (2) and get

$$\begin{aligned}&\mathrm{P}(D_{\Delta t}, t_{\tilde{m}_k}, \xi_{\tilde{M}}|\Delta t, d, \tilde{m}_k, \tilde{M})\\ &\propto \mathrm{P}(\Delta t|D_{\Delta t}, t_{\tilde{m}_k}, \xi_{\tilde{M}}, \tilde{m}_k, \tilde{M})\\ &\quad\cdot \mathrm{P}(D_{\Delta t})\mathrm{P}(t_{\tilde{m}_k}|\tilde{m}_{bfk}, \tilde{M})\mathrm{P}(d|\xi_{\tilde{M}}, \tilde{M})\mathrm{P}(\xi_{\tilde{M}}|\tilde{M})\\ &\approx \mathrm{P}(\Delta t|D_{\Delta t}, t_{\tilde{m}_k}, \xi_{\tilde{M}}, \tilde{m}_k, \tilde{M})\\ &\quad\cdot \mathrm{P}(D_{\Delta t})\mathrm{P}(t_{\tilde{m}_k}|\tilde{m}_k, \tilde{M})\mathrm{P}(\xi_{\tilde{M}}|d, \tilde{M}),\end{aligned} \tag{5}$$

where the likelihood, assuming a Gaussian distribution, can be expressed as

$$\begin{aligned}&\mathrm{P}(\Delta t|D_{\Delta t}, t_{\tilde{m}_k}, \xi_{\tilde{M}}, \tilde{m}_k, \tilde{M})\\ &= \prod_{i,i<j}^{N_{\rm im}} \frac{1}{\sqrt{2\pi}\sigma_{\Delta t_{ij}}} \exp\left[-\frac{(\Delta t_{ij} - \Delta t^{\rm P}_{ij,\tilde{m}_k})^2}{2\sigma^2_{\Delta t_{ij}}}\right],\end{aligned} \tag{6}$$

where j represents the reference lensed image in the time-delay modelling,[5] Δt_{ij} represents the measured time delays between lensed images i and j, $\Delta t^{\rm P}_{ij,\tilde{m}_k}$ represents the predicted time delays, and $\sigma_{\Delta t_{ij}}$ is the 1σ uncertainties of the time-delay measurement. The predicted time delays in equation (6) can be expressed as

$$\Delta t^{\rm P}_{ij,\tilde{m}_k} = \underbrace{(D_{\Delta t}/c)\Delta\tau_{ij}}_{\text{cosmological time delays}} + \underbrace{t_{i,\tilde{m}_k} - t_{j,\tilde{m}_k}}_{\text{microlensing time delays}}, \tag{7}$$

where $\Delta\tau_{ij}$ is the difference of the Fermat potential at image i and image j, and c is the speed of light. The approximation in equation (5) is valid because $\xi_{\tilde{M}}$ is mainly determined by d, as long as there is an arc or ring due to the lensed emission of the host galaxy of the background AGN. Because we are interested in $D_{\Delta t}$ given the microlensing model $\tilde{m}_k$, we can marginalize $t_{\tilde{m}_k}$ and $\xi_{\tilde{M}}$ in equation (2) to obtain

$$\begin{aligned}&\mathrm{P}(D_{\Delta t}|\Delta t, d, \tilde{m}_k, \tilde{M})\\ &= \int\int \mathrm{d}t_{\tilde{m}_k}\mathrm{d}\xi_{\tilde{M}}\mathrm{P}(D_{\Delta t}, t_{\tilde{m}_k}, \xi_{\tilde{M}}|\Delta t, d, \tilde{m}_k, \tilde{M}).\end{aligned} \tag{8}$$

To conservatively estimate the posterior of $D_{\Delta t}$, we should marginalize all over different microlensing models caused by different accretion disc configurations and microlensing patterns,

$$\mathrm{P}(D_{\Delta t}|\Delta t, d, \tilde{M}) = \int \mathrm{d}\tilde{m}_k \mathrm{P}(D_{\Delta t}|\Delta t, d, \tilde{m}_k, \tilde{M})\mathrm{P}(\tilde{m}_k), \tag{9}$$

where $\mathrm{P}(\tilde{m}_k)$ is the prior on the configuration of the accretion disc. In this paper, we simply set a flat prior on the different configurations listed in Section 2 to demonstrate this method. Thus, equation (9) can be approximated as

$$\mathrm{P}(D_{\Delta t}|\Delta t, d, \tilde{M}) \approx \frac{1}{N}\sum_{\tilde{m}_k} \mathrm{P}(D_{\Delta t}|\Delta t, d, m_k, \tilde{M}), \tag{10}$$

where N is the number of configurations.

4 TIME-DELAY MODELLING

Since the microlensing time-delay effect is an absolute, rather than fractional, error, lens systems with short time delays are expected to be affected more. Therefore, we study the impact of the microlensing time-delay effect on two quadruply lensed systems, PG 1115+080 as the example with short time delays, in Section 4.1, and RXJ 1131−1231 as the example with long time delays, in Section 4.2.

4.1 PG1115+080

The PG 1115+080 source quasar, with a redshift of $z_{\rm s} = 1.722$, is quadruply lensed by a galaxy with $z_{\rm d} = 0.31$ (Henry & Heasley 1986; Christian, Crabtree & Waddell 1987; Tonry 1998). Among the four quasar images is an image pair A_1 and A_2 near the critical curve. As the image pair has too small a separation to be properly resolved in the seeing-limited monitoring observations, the COSMOGRAIL monitoring campaign can only obtain three light curves (*A* light curve: the combined light curve of A_1 and A_2, *B* light curve, and *C* light curve; see B18 in detail), which yields two time-delay measurements, Δt_{AC} and Δt_{BC}.[6] We thereby need to carefully use the information from the data and prevent using the same information twice (i.e. set $\Delta t_{A_1C} = \Delta t_{A_2C} = \Delta t_{AC}$).

If the difference of the Δt_{A_1C} and Δt_{A_2C} delays in the combined light curve is large enough, we can separate the measurements by doing an autocorrelation analysis on the combined light curve, which can reveal a second peak in the autocorrelation curve (see e.g. fig. 3 in Cheung et al. 2014). If, on the other hand, the delay is too small and especially the quality of data is not good enough, the delay is indistinguishable in the combined light curve (see B18). Therefore, the total predicted time delay between *A* and *C* could be approximately expressed as

$$\Delta t^{\rm P}_{AC,\tilde{m}_k} \approx \frac{F_{A_1}}{F_{A_1}+F_{A_2}}\Delta t^{\rm P}_{A_1C,\tilde{m}_k} + \frac{F_{A_2}}{F_{A_1}+F_{A_2}}\Delta t^{\rm P}_{A_2C,\tilde{m}_k}, \tag{11}$$

where F_{A_1} and F_{A_2} are the fluxes of the A_1 and A_2 lensed quasars, respectively.[7] Therefore, the log-likelihood of equation (6) is

$$\begin{aligned}&-\ln\mathrm{P}(\Delta t|D_{\Delta t}, t_{\tilde{m}_k}, \xi_{\tilde{M}}, \tilde{m}_k, \tilde{M})\\ &= \frac{\left(\Delta t_{AC} - \Delta t^{\rm P}_{AC,\tilde{m}_k}\right)^2}{2\sigma^2_{\Delta t,AC}} + \frac{\left(\Delta t_{BC} - \Delta t^{\rm P}_{BC,\tilde{m}_k}\right)^2}{2\sigma^2_{\Delta t,BC}} + \text{const},\end{aligned} \tag{12}$$

where 'const' is for normalization.

Note that we use equations (11) and (12) in the analysis of a quad system with only two measured time delays. Equation (6) should be used in a more general scenario.

B18 use PyCS, a PYTHON curve-shifting toolbox containing state-of-the-art curve-shifting techniques (Tewes et al. 2013b; Bonvin et al. 2016), to analyse the three data sets in the different epochs (see Fig. 2):

(i) PyCS-Schechter: B18 use PyCS to reanalyse the data set that was obtained with the Hiltner, WIYN, NOT, and Du Pont telescopes in 1996–1997 (Schechter et al. 1997).

(ii) PyCS-Maidanak+Mercator: B18 use PyCS to reanalyse the data that was obtained at the Maidanak telescope in 2004–2006 (Tsvetkova et al. 2010) and the Mercator telescope in 2006–2009.

(iii) PyCS-WFI: B18 use PyCS to analyse the data set that was recently obtained with the ESO MPIA 2.2m telescope between 2016 December and 2017 July.

[5] Using the full covariance matrix of time-delay measurements is still under development, and beyond the scope of this paper.

[6] We choose *C* as the reference image because Δt_{AC} and Δt_{BC} are the two tightest constraints. Note that the errors of there two delays are correlated.

[7] The uncertainties on $F_{A_1}/(F_{A_1}+F_{A_2})$ and $F_{A_2}/(F_{A_1}+F_{A_2})$ are small enough that we can approximate them as ≈0.

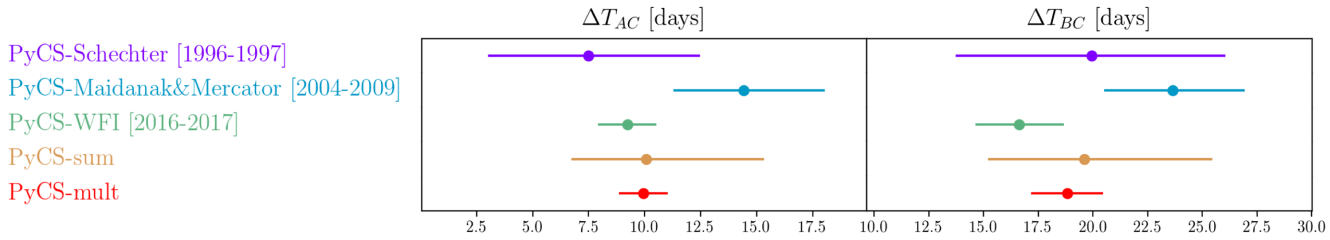

Figure 2. The comparison of the time-delay measurements in different epochs by using the PyCS curve-shifting algorithm (see details in B18). PyCS-Schechter [1996–1997] is computed using the Schechter data set obtained in 1996–1997, PyCS-Maidanak+Mercator [2004–2009] is computed using the Maidanak and Mercator data set in 2004–2009, PyCS-WFI [2016–2017] is computed using the WFI data set obtained in 2016–2017. 'PyCS-sum' refers to the marginalization over the three data sets and 'PyCS-mult' refers to the joint set of estimates. The mean values and error bars are, respectively, the 50th, 16th, and 84th percentiles of the associated time-delay probability distributions.

(iv) 'PyCS-sum' refers to the marginalization over the three data sets.

(v) 'PyCS-mult' refers to the joint set of estimates.

In Section 4.1.1, we initially use PyCS-mult as input time delays and show the posterior of $D_{\Delta t}$ and $t_{\tilde{m}_k}$ under different source configurations as well as $D_{\Delta t}$ after marginalizing over different source configurations. In Section 4.1.2, however, we argue that we should model the three time-delay measurements (PyCS-Schechter, PyCS-Maidanak+Mercator, and PyCS-WFI) simultaneously rather than using PyCS-mult.

4.1.1 Constraining the microlensing effect and time-delay distance simultaneously

In this section, we use the PyCS-mult values ($\Delta t_{AC} = 9.9^{+1.1}_{-1.1}$ d and $\Delta t_{BC} = 18.8^{+1.6}_{-1.6}$ d) in Fig. 2 to represent the most common situation, that is one in which we only have a time-delay data set from a single epoch. In equation (5), since the $\xi_{\tilde{M}}$ is dominated by the lens imaging (up to the MST), we can decouple the lens imaging modelling process and the time-delay modelling process. While the details of the lens imaging modelling are important for measuring H_0, in this paper we focus instead on demonstrating the new time-delay-modelling method developed in Section 3 and present the constraint on the blinded $D_{\Delta t}$[8] and the microlensing time delays.

Fig. 3 shows the posteriors of the constraints on the microlensing time delays and blinded $D_{\Delta t}$ with selected accretion disc configurations. The most constraining case (or the case with tightest prior on microlensing time delays), that is with size $= 0.5R_0$, $\phi = 0^\circ$, and PA $=0^\circ$, provides the best constraint on $D_{\Delta t}$. In Fig. 4, we show the fractional difference of $D_{\Delta t}$. In panel (a), the top curve represents the case that ignores the microlensing time-delay effect and the two bottom curves represent the cases in which (1) we convolve the probability distribution of the loosest constraint of microlensing (size $= 2R_0$, $\phi = 60^\circ$, and PA $=0^\circ$) with the probability distribution of the observed time delays, and (2) we simply add the uncertainty of the case with the loosest constraint on microlensing to the observed time-delay uncertainty in quadrature and shift the mean of the observed time delay by the mean of the loosest case. In both cases, the constraints on $D_{\Delta t}$ are all looser than our method because both of them ignore the information from the cosmological time-delay ratios. The rest of the curves show the results in all different accretion disc configurations. Panel (a) provides two insights. First, the peaks gradually shift to larger $D_{\Delta t}$ when we increase the disc size. This makes sense as the larger the accretion disc is, the more positive the mean of the microlensing time-delay effect is (TK18). Secondly, the size of the accretion disc dominates the uncertainty of the inferred $D_{\Delta t}$. Panel (b) shows the result that marginalizes all the different accretion disc configurations from panel (a).

[8]We will unblind the results *only after* coming to a consensus among the coauthors that we think we have eliminated all systematic errors, and publish the value of H_0 in Chen et al. (2018b, in preparation) without any modification. This is an important step to avoid confirmation bias (Plous 1993).

4.1.2 The discrepant time-delay measurements in the different epochs

Even though the TDC has showed that the current PyCS curve-shifting technique can remove the contamination from the 'standard' microlensing magnification effect and accurately measure time delays, PyCS-WFI and PyCS-Maidanak are $>1\sigma$ discrepant (see PyCS-Maidanak+Mercator, and PyCS-WFI in Fig. 2). Thus, before TK18, this raised the question of how to combine the measurements .

(i) First, we consider that we can measure the same cosmological delays on the three data sets, in which case we have three independent measurements of the delay that can be combined by multiplying their probability distribution functions. This is the PyCS-mult estimate in Fig. 2.

(ii) Secondly, we consider that microlensing is biasing our measurements on each data set, in which case the combined estimate is obtained by marginalizing over the three measurements because we do not have information about the microlensing time-delay effect. This is the PyCS-sum in Fig. 2.

Under the assumptions of TK18, the discrepancy in the time-delay measurements in the different epochs can be understood, as the microlensing time-delay effect can vary across 10 to 20 yr (e.g. Schechter & Wambsganss 2002; Mosquera & Kochanek 2011). Therefore, we should use neither PyCS-mult nor PyCS-sum. Instead, to deliver an unbiased $D_{\Delta t}$ measurement and make good use of information from the microlensing time-delay maps and the cosmological time-delay ratios, it is better to model each time-delay measurement with its own microlensing parameter sets. That

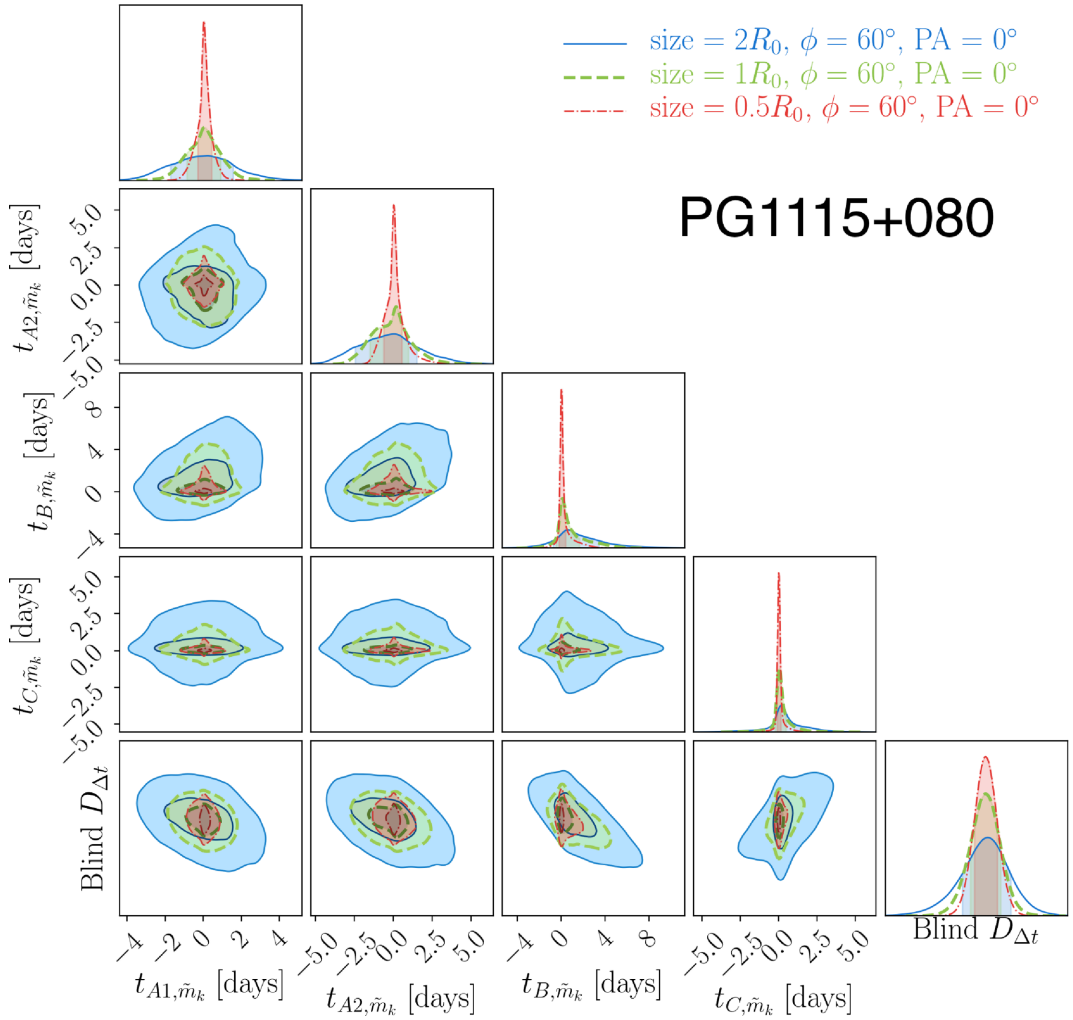

Figure 3. Example showing the posteriors of the microlensing time-delay parameters at each lensed image given different sizes but the same ϕ and PA of the accretion disc. The results show that the smaller the disc size is, the tighter the $D_{\Delta t}$ is. We show the results with all the disc configurations we considered in Fig. 4. The shaded regions in the marginalized one-dimensional probability distribution functions represent the 1σ uncertainty.

is, equation (5) should be expanded to

$$\begin{aligned}
&\mathrm{P}(D_{\Delta t}, t_{S,\tilde{m}_k}, t_{M,\tilde{m}_k}, t_{W,\tilde{m}_k}, \xi_{\tilde{M}}|\Delta t_S, \Delta t_M, \Delta t_W, d, \tilde{m}_k, \tilde{M}) \\
&\quad \approx \mathrm{P}(\Delta t_S, \Delta t_M, \Delta t_W|D_{\Delta t}, t_{S,\tilde{m}_k}, t_{M,\tilde{m}_k}, t_{W,\tilde{m}_k}, \xi_{\tilde{M}}, \tilde{m}_k, \tilde{M}) \\
&\qquad \cdot \mathrm{P}(D_{\Delta t})\mathrm{P}(t_{S,\tilde{m}_k}, t_{M,\tilde{m}_k}, t_{W,\tilde{m}_k}|\tilde{m}_k, \tilde{M})\mathrm{P}(\xi_{\tilde{M}}|d, \tilde{M}),
\end{aligned} \tag{13}$$

where

$$\begin{aligned}
&\mathrm{P}(t_{S,\tilde{m}_k}, t_{M,\tilde{m}_k}, t_{W,\tilde{m}_k}|\tilde{m}_k, \tilde{M}) \\
&\quad = \mathrm{P}(t_{S,\tilde{m}_k}|\tilde{m}_k, \tilde{M})\mathrm{P}(t_{M,\tilde{m}_k}|\tilde{m}_k, \tilde{M})\mathrm{P}(t_{W,\tilde{m}_k}|\tilde{m}_k, \tilde{M}) \\
&\quad = \prod_i^{N_{\rm im}} \mathrm{P}(t_{S,i,m_k}|\tilde{m}_k, \tilde{M}) \prod_i^{N_{\rm im}} \mathrm{P}(t_{M,i,m_k}|\tilde{m}_k, \tilde{M}) \\
&\qquad \cdot \prod_i^{N_{\rm im}} \mathrm{P}(t_{W,i,m_k}|\tilde{m}_k, \tilde{M}),
\end{aligned} \tag{14}$$

and the likelihood is

$$\begin{aligned}
&\mathrm{P}(\Delta t_S, \Delta t_M, \Delta t_W|D_{\Delta t}, t_{S,\tilde{m}_k}, t_{M,\tilde{m}_k}, t_{W,\tilde{m}_k}, \xi_{\tilde{M}}, \tilde{m}_k, \tilde{M}) \\
&\quad = \prod_{i,i<j}^{N_{\rm im}} \frac{1}{\sqrt{2\pi}\sigma_{\Delta t_{S,ij}}} \exp\left[-\frac{(\Delta t_{S,ij} - \Delta t^{\rm P}_{S,ij,\tilde{m}_k})^2}{2\sigma^2_{\Delta t_{S,ij}}}\right] \\
&\qquad \cdot \prod_{i,i<j}^{N_{\rm im}} \frac{1}{\sqrt{2\pi}\sigma_{\Delta t_{M,ij}}} \exp\left[-\frac{(\Delta t_{M,ij} - \Delta t^{\rm P}_{M,ij,\tilde{m}_k})^2}{2\sigma^2_{\Delta t_{M,ij}}}\right] \\
&\qquad \cdot \prod_{i,i<j}^{N_{\rm im}} \frac{1}{\sqrt{2\pi}\sigma_{\Delta t_{W,ij}}} \exp\left[-\frac{(\Delta t_{W,ij} - \Delta t^{\rm P}_{W,ij,\tilde{m}_k})^2}{2\sigma^2_{\Delta t_{W,ij}}}\right],
\end{aligned} \tag{15}$$

where the subscripts 'S', 'M', and 'W' represent the time-delay measurements from PyCS-Schechter, PyCS-Maidanak+Mercator, and PyCS-WFI, respectively. Equation (15) means that we have six measurements (two for each data set) to constrain one $D_{\Delta t}$ and three sets of independent microlensing parameters (see Fig. 5). We assume the three data sets share the same accretion disc configuration, $\tilde{m}_k$, because the configuration of the accretion disc should stay invariant over the 20 yr. We also follow equation (9) to

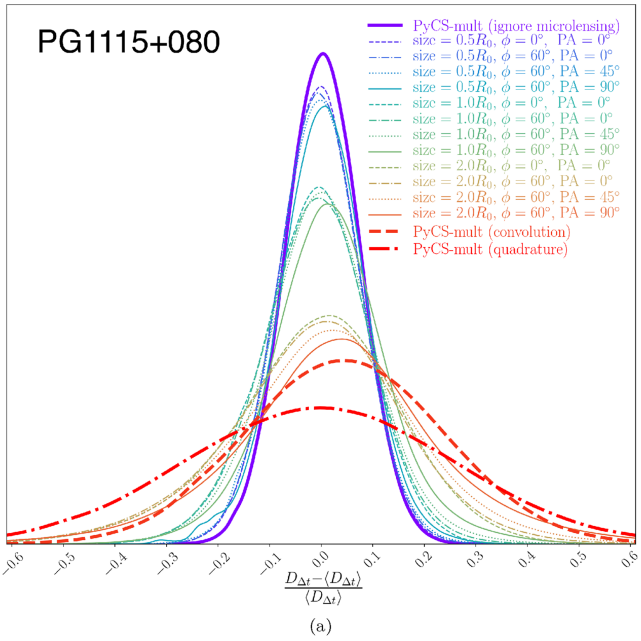

Figure 4. The fractional difference of $D_{\Delta t}$ in different conditions. In panel (a), the top curve shows the case that ignores the microlensing effect; the two curves at the bottom represent the cases in which we modify the PyCS-mult by convolving with the loosest case of microlensing model and by adding the loosest case of microlensing model in quadrature respectively, and the rest are the results with different accretion disc configurations. In panel (b), the top curve shows the case that ignores the microlensing effect (7.3 per cent) and the bottom curve shows the constraint on $D_{\Delta t}$ after we marginalize the different accretion discs listed in Section 2 (11.3 per cent). The shaded regions and percentages represent the 1σ uncertainties.

marginalize all the different source configurations and show the results in Table 2 and Fig. 6. Table 2 shows the inferred probability distribution of the microlensing time-delay parameters at the position of each lensed image in different data sets. Fig. 6 shows the different $D_{\Delta t}$ values when we adopt PyCS-sum and 'PyCS-Schechter&PyCS-Madanak+Mercator&PyCS-WFI'. Note that 'PyCS-Schechter&PyCS-Madanak+Mercator&PyCS-WFI' indicates that we use three different microlensing parameter sets to model three different time-delay measurements.

4.2 RXJ1131-1231

The RXJ 1131−1231 system is a quadruply lensed quasar discovered by Sluse et al. (2003), who also measured the spectroscopic redshifts of lensing galaxy and the background source to be at $z_{\rm d} = 0.295$ and $z_{\rm s} = 0.658$. Because of the long time delays (∼90.5 d) of this lens system, Tewes et al. (2013b) can measure the time delay of image D, with a fractional uncertainty of 1.5 per cent (1σ), while the delays between the three close images A, B, and C are compatible with being 0 d (i.e. $\Delta_{BA} = 0.5 \pm 1.5$ d, $\Delta_{CA} = -0.5 \pm 1.5$ d, $\Delta_{DA} = 90.5 \pm 1.5$ d). Therefore, for RXJ 1131−1231, equation (6) can be expressed as

$$
\begin{aligned}
&\mathrm{P}(\Delta t | D_{\Delta t}, t_{\tilde{m}_k}, \xi_{\tilde{M}}, \tilde{m}_k, \tilde{M}) \\
&= \frac{1}{\sqrt{2\pi}\sigma_{\Delta t_{BA}}} \exp\left[-\frac{(\Delta t_{BA} - \Delta t^{\rm P}_{BA,\tilde{m}_k})^2}{2\sigma^2_{\Delta t_{BA}}}\right] \\
&\cdot \frac{1}{\sqrt{2\pi}\sigma_{\Delta t_{CA}}} \exp\left[-\frac{(\Delta t_{CA} - \Delta t^{\rm P}_{CA,\tilde{m}_k})^2}{2\sigma^2_{\Delta t_{CA}}}\right] \\
&\cdot \frac{1}{\sqrt{2\pi}\sigma_{\Delta t_{DA}}} \exp\left[-\frac{(\Delta t_{DA} - \Delta t^{\rm P}_{DA,\tilde{m}_k})^2}{2\sigma^2_{\Delta t_{DA}}}\right] . \qquad (16)
\end{aligned}
$$

We use the same κ, γ, and $\kappa_\star/\kappa$ as TK18 to generate the microlensing time-delay maps given the combinations of different accretion disc sizes ($0.5R_0$, $1R_0$, and $2R_0$), different ϕ to the line of slight (0° and 30°), and different PA (0°, 45°, and 90°) at the four lensed images. We show the constraint on $D_{\Delta t}$ in different accretion disc configurations in Fig. 7 and the marginalized posteriors of the microlensing time delays in Table 3. As expected, the microlensing time-delay effect on the lens with longer time delays has less impact. In the case of RXJ 1131−1231, the impact by the microlensing time-delay effect is negligible.

5 CONCLUSIONS

This paper quantifies the impact of microlensing time delays, produced under the assumption that AGN variability is the lamp-post type, on the time-delay distance. For that purpose, we calculate the time-delay distance, $D_{\Delta t}$, including the microlensing time-delay effect for two lens systems, PG 1115+080 and RXJ 1131−1231, We find that this broadens the probability distribution by about 3 per cent in the case of PG 1115+080 and 0.1 per cent in the case of RXJ 1131−1231.

Given the lamp-post model assumption, although we do not have any knowledge about how severely each light curve is affected by the microlensing time-delay effect, the cosmological time-delay ratios, which are well-constrained by the full surface brightness morphology of the lensed host galaxy emission, provide the constraining information on the possible combinations of the microlensing time delay at each lensed image position. Furthermore, the microlensing time-delay maps also provide constraints on the microlensing time-delay effect at each lensed image position. Thus, we have developed a new time-delay prediction model, which uses the information from cosmological time-delay ratios, as well as the information from microlensing time-delay maps, to remove the biases caused by this proposed effect under a Bayesian framework.

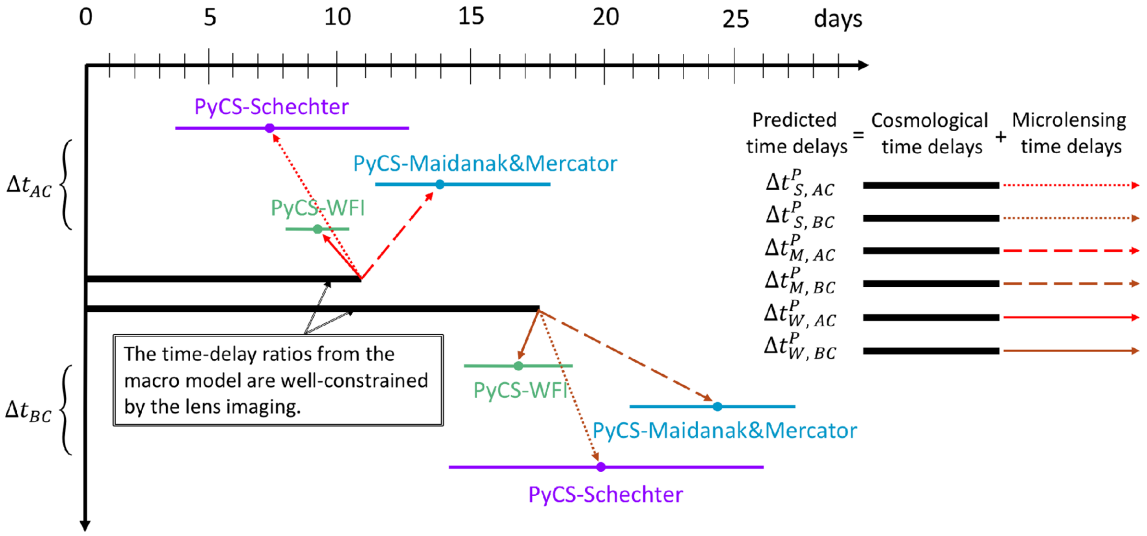

Figure 5. This figure illustrates the idea of simultaneously fitting six different time-delay measurements with a single $D_{\Delta t}$ and three independent sets of microlensing parameters given the prior from the lens imaging. PyCS-Shechter, PyCS-Maidanak+Mercator, and PyCS-WFI represent the three time-delay measurements on Δt_{AC} and three time-delay measurements on Δt_{BC} in different epochs. Since the full surface brightness of the multiple lensed images provides a strong constraint on the ratio of the Fermat potential, given a $D_{\Delta t}$ and the lens imaging, we can predict the cosmological time delays (two thick black horizontal lines). On top of the cosmological time delays, given $t_{S,\tilde{m}_{\mathbf{k}}}$, $t_{M,\tilde{m}_k}$, $t_{W,\tilde{m}_k}$ (i.e. the three independent microlensing parameter sets), we can obtain three sets of predicted time-delays, $\Delta t^{\rm P}_{S,ij}$, $\Delta t^{\rm P}_{M,ij}$, $\Delta t^{\rm P}_{W,ij}$ (i.e. the six predicted time delays listed on the right-hand side) and use the observed time delays to constrain the $D_{\Delta t}$ and the microlensing time delays. The mean values and error bars are respectively the 50th, 16th, and 84th percentiles of the associated time-delay probability distributions.

Table 2. The posteriors of the microlensing time delays at each lensed image in different data sets of PG 1115+080. The subscripts *S*, *M*, and *W* represent the results from the Schechter data set, Maidanak+Mercator data set, and WFI data set, respectively. We have marginalized all the accretion disc configurations listed in Section 2. The mean values and error bars are respectively the 50th, 16th, and 84th percentiles.

Parameters	t_{S,A_1}	t_{S,A_2}	$t_{S,B}$	$t_{S,C}$
Time delays (days)	$0.1^{+1.1}_{-1.0}$	0.1 ± 1.7	$0.06^{+1.34}_{-0.94}$	$0.06^{+0.47}_{-0.42}$
Parameters	t_{M,A_1}	t_{M,A_2}	$t_{M,B}$	$t_{M,C}$
Time delays (days)	$0.08^{+1.26}_{-0.88}$	$0.1^{+2.4}_{-1.6}$	$0.12^{+2.45}_{-0.86}$	$0.02^{+0.49}_{-0.41}$
Parameters	t_{W,A_1}	t_{W,A_2}	$t_{W,B}$	$t_{W,C}$
Time delays (days)	$0.07^{+0.82}_{-1.03}$	$0.06^{+0.88}_{-1.59}$	$0.06^{+0.94}_{-0.77}$	$0.07^{+0.66}_{-0.43}$

There are several key results:

(i) Under the assumption of TK18, different lens systems can yield different H_0 due to the fact that the measured time delays are not the cosmological time delays but the combination of cosmological time delays plus microlensing time delays. With this new time-delay prediction model, we can separately predict the cosmological time delays and microlensing time delays to measure an unbiased value of H_0 for each lens. Thus, this paper addresses concerns that TDSL has already hit the systematics floor in the time-delay measurements due to this newly proposed microlensing time-delay effect, although it does increase the error budget.

(ii) The time-delay measurements in different epochs should be modelled by different microlensing parameters as they are likely affected by different microlensing time-delay effects.

(iii) Given a lens system, the constraint on $D_{\Delta t}$ mainly depends on the size of the accretion disc, whereas the inclination and the position angle of the disc have little influence. Thus, the smaller the

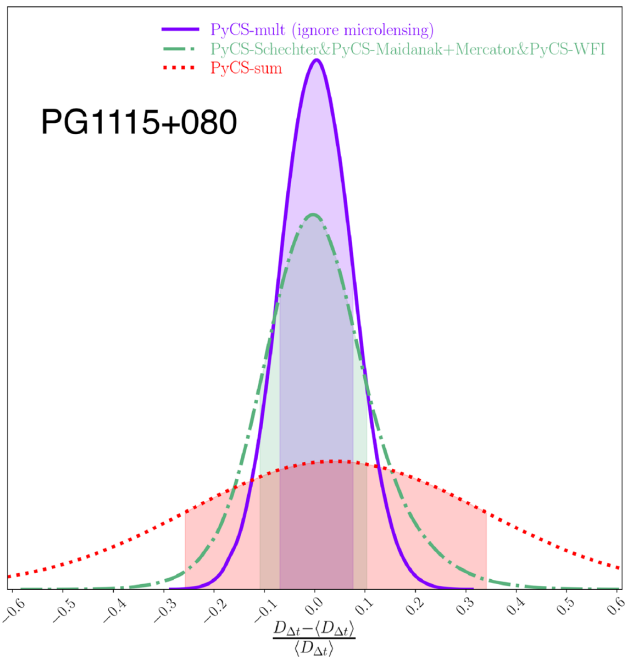

Figure 6. The comparison of the fractional difference of $D_{\Delta t}$ among the case that ignores the microlensing time-delay effect (7.3 per cent), the case that uses PyCS-Schechter&PyCS-Madanak+Mercator&PyCS-WFI (10.4 per cent), and the case that uses PyCS-sum (30 per cent). Note that the last two curves have already marginalized over all different accretion disc configurations. In the case of PG 1115+080, the uncertainty of $D_{\Delta t}$ increases from ∼7 per cent to ∼10 per cent. The shaded regions and the percentages represent the 1σ uncertainties.

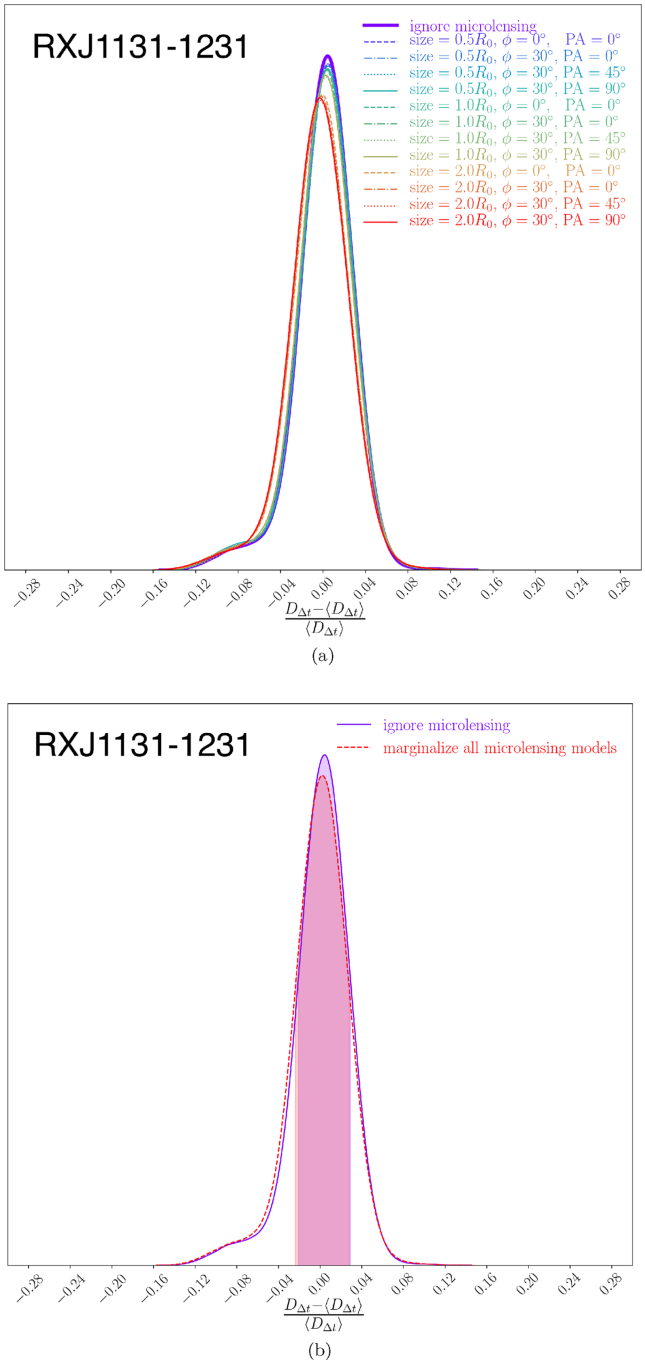

Figure 7. We present the fractional difference of $D_{\Delta t}$ in different conditions for RXJ 1131−1231. In panel (a), the top curve shows the case that ignores the microlensing effect and the rest are the results with different accretion disc configurations. In panel (b), the top curve shows the case that ignores the microlensing effect (2.5 per cent) and the bottom curve shows the constraint on $D_{\Delta t}$ after we marginalize the different accretion discs mentioned in Section 4.2 (2.6 per cent). In the case of RXJ 1131−1231, the microlensing time-delay effect is negligible. The shaded regions and percentages represent the 1σ uncertainties.

disc is, the smaller the variances on the microlensing time delays are.

(iv) The uncertainty on $D_{\Delta t}$ from PG 1115+080, which has relatively short time delays, increases from ∼7 per cent to ∼10 per cent when we include the microlensing time-delay effects. Without our new technique, the uncertainty on $D_{\Delta t}$ from PG 1115+080 can increase by up to 30 per cent.

(v) The uncertainty on $D_{\Delta t}$ from RXJ 1131−1231, which has relatively long time delays, increases only from ∼2.5 per cent to ∼2.6 per cent when we include the microlensing time-delay effects. Thus, the impact of the microlensing time-delay effect on RXJ 1131−1231 is negligible.

Table 3. The posteriors of the microlensing time delays at each lensed image of RXJ 1131−1231. We have marginalized all the accretion disc configurations listed in Section 4.2. The mean values and error bars are respectively the 50th, 16th, and 84th percentiles.

Parameters	t_A	t_B	t_C	t_D
Time delays (days)	$0.02^{+0.40}_{-0.59}$	$0.02^{+0.38}_{-0.20}$	$0.02^{+0.28}_{-0.21}$	$0.01^{+0.15}_{-0.12}$

Note that although we assume the lamp-post model on accretion disc, there is evidence (e.g. Morgan et al. 2010; Blackburne et al. 2011) showing that the size of the accretion disc is larger than the prediction from the standard thin-disc theory. In addition, there exist a variety of alternative accretion disc models (e.g. Beloborodov 1999), including, for example, the inhomogeneous accretion disc (e.g. Dexter & Agol 2011) for which variability is different from the lamp-post model.

As the amplitude of this effect highly depends on the accretion disc models, which are not well understood, in our future determinations of H_0 from the H0LiCOW programme, we will present the measurements both with and without microlensing time-delay effects. The techniques for verifying the accretion disc models by using observational data are currently under development.

Finally, we want to stress that with the advantage of cosmological time-delay ratios, quads are better than doubles in term of constraining the microlensing time-delay effect in measuring the value of H_0. The final H_0 measurements from PG 1115+080 and RXJ 1131−1231 will be presented in Chen et al. (2018b, in prep).

ACKNOWLEDGEMENTS

We thank Cristian E. Rusu and Stefan Hilbert for comments. G. C.-F. C. also thanks Chun-Hao To and Shih-Wei Chuo for technical discussions, and the UC Davis cosmology group for providing a friendly research environment. G. C.-F. C. acknowledges support from the Ministry of Education in Taiwan via Government Scholarship to Study Abroad (GSSA). G. C.-F. C. and C. D. F. acknowledge support from the National Science Foundation under grant AST-1715611. G. C.-F. C. and C. D. F. thank the Max Planck Institute for Astrophysics for kind hospitality during working visits. K.C.W. is supported by an EACOA Fellowship awarded by the East Asia Core Observatories Association, which consists of the Academia Sinica Institute of Astronomy and Astrophysics, the National Astronomical Observatory of Japan, the National Astronomical Observatories of the Chinese Academy of Sciences, and the Korea Astronomy and Space Science Institute. J. C., V. B., M. M., and F. C. are supported by the Swiss National Science Foundation. S. V. has received funding from the European Research Council (ERC) under the European Union's Horizon 2020 research and innovation programme (grant agreement No 758853). L. V. E. K. are supported through an NWO-VICI grant (project number 639.043.308). S. H. S thanks the Max Planck Society for support through the Max Planck Research Group. A. J. S. and T. T. acknowl-

edge support by NASA through STSCI grant HST-GO-15320, and by the Packard Foundation through a Packard Fellowship to T. T.

REFERENCES

Agnello A., 2017, MNRAS, 471, 2013
Agnello A. et al., 2018, MNRAS, 479, 4345
Aubourg É. et al., 2015, Phys. Rev. D, 92, 123516
Avestruz C., Li N., Lightman M., Collett T. E., Luo W., 2017, preprint (arXiv:1704.02322)
Beloborodov A. M., 1999, in Poutanen J., Svensson R., eds, ASP Conf. Ser. Vol. 161, High Energy Processes in Accreting Black Holes. Astron. Soc. Pac., San Francisco, p. 295
Birrer S., Amara A., Refregier A., 2015, ApJ, 813, 102
Birrer S., Welschen C., Amara A., Refregier A., 2017, J. Cosmology Astropart. Phys., 4, 049
Blackburne J. A., Pooley D., Rappaport S., Schechter P. L., 2011, ApJ, 729, 34
Bonvin V., Tewes M., Courbin F., Kuntzer T., Sluse D., Meylan G., 2016, A&A, 585, A88
Bonvin V. et al., 2017, MNRAS, 465, 4914
Bonvin V., et al., 2018, A&A, preprint (arXiv:1804.09183)
Chen G. C.-F. et al., 2016, MNRAS, 462, 3457
Cheung C. C. et al., 2014, ApJ, 782, L14
Christian C. A., Crabtree D., Waddell P., 1987, ApJ, 312, 45
Courbin F. et al., 2018, A&A, 609, A71
de Grijs R., Courbin F., Martínez-Vázquez C. E., Monelli M., Oguri M., Suyu S. H., 2017, Space Sci. Rev., 212, 1743
Dexter J., Agol E., 2011, ApJ, 727, L24
Ding X. et al., 2018, preprint (arXiv:1801.01506)
Dobler G., Fassnacht C., Treu T., Marshall P. J., Liao K., Hojjati A., Linder E., Rumbaugh N., 2013, preprint (arXiv:1310.4830)
Eulaers E. et al., 2013, A&A, 553, A121
Falco E. E., Gorenstein M. V., Shapiro I. I., 1985, ApJ, 289, L1
Fassnacht C. D., Koopmans L. V. E., Wong K. C., 2011, MNRAS, 410, 2167
Fassnacht C. D., Xanthopoulos E., Koopmans L. V. E., Rusin D., 2002, ApJ, 581, 823
Foreman-Mackey D., Hogg D. W., Lang D., Goodman J., 2013, PASP, 125, 306
Freedman W. L., 2017, Nature Astronomy, 1, 0169
Goodman J., Weare J., 2010, CAMCoS, 5, 65
Henry J. P., Heasley J. N., 1986, Nature, 321, 139
Hinshaw G. et al., 2013, ApJS, 208, 19
Hinton S. R., 2016, JOSS, 1, 00045
Jee I., Komatsu E., Suyu S. H., 2015, J. Cosmology Astropart. Phys., 11, 033
Jee I., Komatsu E., Suyu S. H., Huterer D., 2016, J. Cosmology Astropart. Phys., 4, 031
Joseph R. et al., 2014, A&A, 566, A63
Keeton C. R., Moustakas L. A., 2009, ApJ, 699, 1720
Kochanek C. S., Dalal N., 2004, ApJ, 610, 69
Komatsu E. et al., 2011, ApJS, 192, 18
Koopmans L. V. E., 2005, MNRAS, 363, 1136
Koopmans L. V. E., Treu T., Fassnacht C. D., Blandford R. D., Surpi G., 2003, ApJ, 599, 70
Lanusse F., Ma Q., Li N., Collett T. E., Li C.-L., Ravanbakhsh S., Mandelbaum R., Póczos B., 2018, MNRAS, 473, 3895
Liao K. et al., 2015, ApJ, 800, 11
Lin H. et al., 2017, ApJ, 838, L15
Mao S., Schneider P., 1998, MNRAS, 295, 587
Morgan C. W., Kochanek C. S., Morgan N. D., Falco E. E., 2010, ApJ, 712, 1129
Mosquera A. M., Kochanek C. S., 2011, ApJ, 738, 96
Nightingale J. W., Dye S., 2015, MNRAS, 452, 2940
Oguri M., 2010, PASJ, 62, 1017
Oguri M., Marshall P. J., 2010, MNRAS, 405, 2579
Ostrovski F. et al., 2017, MNRAS, 465, 4325
Ostrovski F. et al., 2018, MNRAS, 473, L116
Peng C. Y., Impey C. D., Rix H.-W., Falco E. E., Keeton C. R., Kochanek C. S., Lehár J., McLeod B. A., 2006, New Astron. Rev., 50, 689
Petrillo C. E. et al., 2017, MNRAS, 472, 1129
Planck Collaboration XIII, 2016, A&A, 594, A13
Plous S., 1993, The Psychology of Judgment and Decision Making. McGraw-Hill Education, Available at: https://books.google.com/books?id=xvWOQgAACAAJ
Rathna Kumar S. et al., 2013, A&A, 557, A44
Refsdal S., 1964, MNRAS, 128, 307
Riess A. G. et al., 1998, AJ, 116, 1009
Riess A. G. et al., 2016, ApJ, 826, 56
Rusu C. E. et al., 2017, MNRAS, 467, 4220
Schechter P. L., Morgan N. D., Chehade B., Metcalfe N., Shanks T., McDonald M., 2017, AJ, 153, 219
Schechter P. L., Wambsganss J., 2002, ApJ, 580, 685
Schechter P. L. et al., 1997, ApJ, 475, L85
Schneider P., Sluse D., 2013, A&A, 559, A37
Schneider P., Sluse D., 2014, A&A, 564, A103
Shajib A. J., Treu T., Agnello A., 2018, MNRAS, 473, 210
Shakura N. I., Sunyaev R. A., 1973, A&A, 24, 337
Sluse D. et al., 2003, A&A, 406, L43
Suyu S. H., 2012, MNRAS, 426, 868
Suyu S. H., Chang T.-C., Courbin F., Okumura T., 2018, Space Sci. Rev., 214, 91
Suyu S. H., Marshall P. J., Auger M. W., Hilbert S., Blandford R. D., Koopmans L. V. E., Fassnacht C. D., Treu T., 2010, ApJ, 711, 201
Tewes M., Courbin F., Meylan G., 2013a, A&A, 553, A120
Tewes M. et al., 2013b, A&A, 556, A22
Tie S. S., Kochanek C. S., 2018, MNRAS, 473, 80 TK18
Tihhonova O. et al., 2018, MNRAS, 477, 5657
Tonry J. L., 1998, AJ, 115, 1
Treu T., Koopmans L. V. E., 2002, MNRAS, 337, L6
Treu T., Marshall P. J., 2016, A&A Rev., 24, 11
Tsvetkova V. S. et al., 2010, MNRAS, 406, 2764
Vegetti S., Koopmans L. V. E., 2009, MNRAS, 392, 945
Wambsganss J., 2006, preprint (arXiv:Astrophysics:e-prints)
Warren S. J., Dye S., 2003, ApJ, 590, 673
Weinberg D. H., Mortonson M. J., Eisenstein D. J., Hirata C., Riess A. G., Rozo E., 2013, Phys. Rep., 530, 87
Williams P. R. et al., 2018, MNRAS, 477, L70
Wong K. C. et al., 2017, MNRAS, 465, 4895
Xu D., Sluse D., Schneider P., Springel V., Vogelsberger M., Nelson D., Hernquist L., 2016, MNRAS, 456, 739

This paper has been typeset from a TEX/LATEX file prepared by the author.